Cu supported on various oxides as a candidate catalyst for dry methane reforming in DIR-SOFCs systems

Adrian Mizera [a,*], Patryk Błaszczak [b], Beata Bochentyn [b], Radosław Lach [a], Ewa Drożdż [a]

[a] AGH University of Science and Technology, Faculty of Materials Science and Ceramics, al. Mickiewicza 30, 30-059 Krakow, Poland

[b] Advanced Materials Center, Faculty of Applied Physics and Mathematics, Gdansk University of Technology, ul. Narutowicza 11/12, 80-233 Gdańsk, Poland

HIGHLIGHTS

- Cu was deposited on α-Al_2O_3, γ-Al_2O_3, CeO_2, ZrO_2 and $SrTiO_3$ supports.
- Catalytic activity of Cu on different oxide supports was tested towards DMR reaction.
- 5%Cu on AlO(OH) shows the highest catalytic activity due to the largest SSA.
- Cu–$SrTiO_3$ shows high catalytic activity and selectivity to CO in DMR.
- Cu–$SrTiO_3$ is a good candidate for DIR-SOFC.

GRAPHICAL ABSTRACT
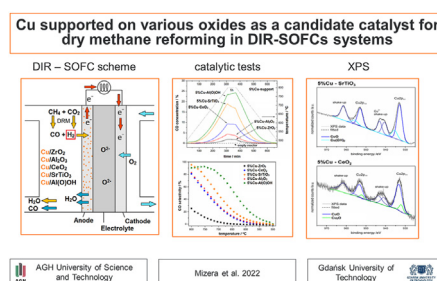
ARTICLE INFO

ABSTRACT

A series of Cu-support systems were tested as potential candidates for DIR-SOFC (Direct Internal Reforming SOFC) catalysts towards a dry reforming of methane (DRM). The various supports (α-Al_2O_3, CeO_2, ZrO_2, $SrTiO_3$) with comparable specific surface area (SSA), and additionally γ-Al_2O_3 with SSA an order of magnitude larger than that of the other supports has been applied. The obtained Cu-support systems were characterized in terms of structure (XRD, XPS), microstructure (SEM), redox properties (TPR/TPOx), and next their catalytic activity and selectivity in DRM reaction were tested. All Cu-support materials show catalytic activity in DRM reaction, but only activity of Cu–$SrTiO_3$ is high (due to the incorporation of Cu into $SrTiO_3$ structure). The catalytic activity of other materials depends on the copper oxidation state (Cu^{2+} and Cu^+). The highest catalytic activity in DRM process

* *Corresponding author.*
  E-mail address: amizera@agh.edu.pl (A. Mizera).

Cu−ZrO$_2$

Cu−SrTiO$_3$

DIR-SOFC

was obtained for Cu−AlO(OH) catalyst thanks to an order of greater SSA than in the case of other systems.

Introduction

Nowadays, hydrogen production in electrochemical devices within internal biogas reforming is one of the most important areas of energy technology development. Using biogas as a fuel in e.g. Solid Oxide Fuel Cells fits perfectly into the concept of distributed energy as these cells could serve as a stationary power source at landfills, farms, etc. However, the widespread use of this kind of technology forces effort to improve the economic viability of such solutions. At the moment, the commercial fuel cells with Ni-YSZ (YSZ − yttria stabilized zirconia) anode are optimized for operating with hydrogen as a fuel. In contrast, the investment cost associated with the installation of the system and the problem of degradation of the cells under the influence of carbon deposition and sulfur poisoning restricts the application of SOFCs directly fueled by bioga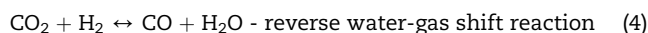s on a large scale. Therefore, effective catalysts allowing to minimize these problems in Direct Internal Reforming Solid Oxide Fuel Cells (DIR-SOFCs) are strongly desirable. Two potential paths may be considered: modifying the existing commercial SOFC anodes by depositing additional catalytic layers on its surface or fabricating novel anode materials containing additional catalytic phase in the structure. The most effective catalysts for reforming reactions are noble metals (Ru, Rh, Pt, Ir), which achieve high catalytic activity towards DRM reaction with relatively low noble metal content [1−5]. Due to the high price and low abundance of the noble metals, attempts to replace them with not so expensive, d-block metals were made. Among them, the best alternative from a catalytic activity point of view is nickel [6−12]. However, nickel is at the same time a good catalyst for the competitive reaction of hydrocarbons reduction to carbon [13,14]. Thus, it is the source of carbon deposit which, by leaving on the active centers of the catalyst, leads to its deactivation [15,16]. The papers from recent years indicate that copper is a less effective catalyst in methane reforming than nickel, but does not cause coking of the material [17,18]. In case of copper, the research is focused mainly on the study of bimetallic catalysts containing Cu [19−23], or the copper incorporated in the mixed oxide structure [24]. However, there is a lack of papers on the catalytic activity of the catalysts containing only copper as an active metal for such applications. The copper was subjected to catalytic properties studies in the WGSR (Water-Gas Shift Reaction) [25], which is frequently considered when analyzing the DRM process. It is not, however, the same reaction and moreover SiO$_2$-based materials is unappropriate for the application in SOFC technology. Our recent paper [26] provides the results of catalytic tests towards DRM reaction systems based on Cu-doped SrTiO$_3$, but there are still no articles in which classic catalytic systems such as catalytically active metal deposited on an oxide support were tested. Nowadays, the dry reforming of methane (DRM) (CH$_4$ + CO$_2$ → CO + H$_2$) became one of the most often studied processes as a test reaction to determine the feasibility of the biogas reforming reaction in electrochemical devices. However, this reaction can be accompanied by numerous parallel and subsequent (often undesirable) reactions at the operating temperatures of these devices. These reactions lead, *inter alia*, to the formation of a carbon deposit (Eqs. (1)−(3)) or substrates for its formation (Eqss. (4) and (5)):

$$2CO \leftrightarrow C_{(s)} + H_2O \text{ - Boudouard reaction} \tag{1}$$

$$CO + H_2 \leftrightarrow C_{(s)} + H_2O - CO \text{ reduction} \tag{2}$$

$$CH_4 \leftrightarrow C_{(s)} + 2H_2 \text{ - pyrolysis of methane} \tag{3}$$

$$CO_2 + H_2 \leftrightarrow CO + H_2O \text{ - reverse water-gas shift reaction} \tag{4}$$

$$CH_4 + H_2O \leftrightarrow CO + 3H_2 \text{ - steam reforming of methane} \tag{5}$$
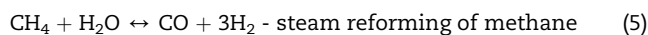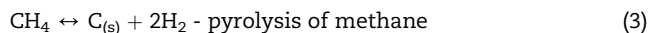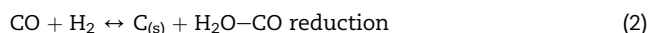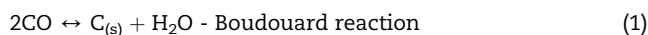
The use of copper in place of nickel in DRM reaction significantly eliminates the above-mentioned, secondary reactions. Based on the previous works [27−30], we can divide the DRM reaction mechanism into four steps. In the first step, the methane species are adsorbed on the catalysts surface followed by dehydrogenation (CH$_4^•$→CH$_3^•$ →CH$_2^•$→CH$^•$→C$^•$). In the next step, the CO$_2$ molecules form CO* species by deoxidation path (CO$_2$•→CO•+O•) or by reaction with hydrogen (CO$_2^•$+H$^•$→COOH$^•$→CO$^•$+OH$^•$). In the third step, the oxidation of CH* and C* species occur resulting in production of various intermediate species in the C−H−O system (CHO$^•$, COH$^•$, CHOH$^•$). These intermediates then form the CO$^•$ and H$^•$ species during the third step of the reaction. Generally, during second and third step, the CO product is formed. In the last step, the hydrogen is generated from the H$^•$ species (H$^•$+H$^•$→H$_2^•$) and water (as a by-product) is generated from the remaining H$^•$ and OH$^•$ species. Nickel as a catalyst is responsible for lowering the activation energy of individual dehydrogenation stages in the DRM process.

As mentioned above, the scientific considerations on the Cu activity in DRM reaction were mostly limited to the area of bimetallic alloys with Cu, the Ni−Cu alloys in particular. In the work [17] Chatla et al. calculated the adsorption energies of carbon on the surfaces of Ni−Cu alloys deposited on γ-Al$_2$O$_3$ with different Ni to Cu ratio. They observed that addition of Cu to Ni results in an increase of the adsorption energy of carbon and thus lower affinity of carbon to adsorption on Ni−Cu alloys. On the other hand, they observed that in case of Ni−Cu alloys with high Cu content (Ni:Cu ratio was 3:1), the

activation energies of individual dehydrogenation steps increase. These results confirm that copper is less effective catalyst in DRM process than nickel catalyst but Cu significantly reduced deposition of carbon.

The use of an appropriate catalyst is one of the basic requirements for effective methane reforming; however, the selection of the support due to the use of the entire system is most often dictated by the electrical properties of this support. The fulfilment of such requirements is particularly important in the context of using a specific material (catalyst-support composite) in electrochemical devices, for example, those devices that are to be used in technologies dedicated to energy conversion. Thus, it was decided to compare in this work on a series of Cu-support materials, where various oxides were selected as supports. These oxides are used in medium- and high-temperature electrochemical devices as conductors with ionic conductivity (ZrO_2, CeO_2), mixed ionic-electronic conductivity ($SrTiO_3$, CeO_2) or isolator (Al_2O_3). The alumina in the form of α-Al_2O_3 or γ-Al_2O_3 is used frequently as a catalytic support material due to its chemical resistance and stability over a wide temperature range. ZrO_2 owes its electrical properties to the ability to transport of O^{2-} ions through a vacancy mechanism [31–33], CeO_2 exhibits a high electronic conductivity component due to the reduction reaction of Ce^{4+} $\rightarrow Ce^{3+}$ in hydrogen atmosphere [34–36] while appropriately doped $SrTiO_3$ shows mixed ionic-electronic conductivity [37–39]. In recent years, the latter two have been of particular interest to scientists who study energy conversion and storage devices. The research confirms that the catalytic activity of the catalyst may depend not only on the size of its particles and its specific surface area (which depends on the surface of the support) but also on the interactions of active metal with the support material [40–42]. The problem of the interactions of the support with the copper catalyst as a catalyst active in hydrogenation reactions, in the water gas shift reaction process or in methanol synthesis, was considered in detail by Chatterjee et al. [43]. The authors of this work, using the methods of temperature programmed hydrogen desorption (H_2-TPD) and reactive frontal chromatography by nitrous oxide (N_2O-RFC) determined the nature of the interaction between Cu and the following supports: carbon (various types), SiO_2, CeO_2, TiO_2, ZnO, Ga_2O_3, Al_2O_3 and MgO. The conclusion of this paper was that the reducible oxides support increased adsorption of oxygen from N_2O and decreased adsorption of hydrogen. The opposite trend, in general prevails in the case of the irreducible (such as Al_2O_3, Gd_2O_3 or MgO) oxides. Therefore, it can be expected that the copper catalyst deposited on reducible supports should support the dehydrogenation reactions and thus also the DRM process. In the case of carbon as a support, no difference was observed between the ratio of N_2O to H_2 (in the N_2O-RFC and H_2-TPD measurements) compared to the measurements made on pure copper as a reference material and the differences in the catalytic activity of this type of materials are the result of large differences in Cu particle sizes distributed over different types of coals. The authors of this work did not present the results of catalytic tests for any reaction, so their valuable research has not been verified in terms of application.

Therefore, taking into account the growing interest in alternative hydrogen sources and their use in fuel cells, we decided to compare the effectiveness of various, often used in electrochemical devices, supports for an active copper metal to form catalysts towards the DRM reaction.

We believe that by this approach we will contribute to the knowledge about the catalytic properties of copper in DRM reaction. Moreover, due to the high importance of the specific surface area of the supports, the tested materials had comparable specific surface area to minimize the influence of this factor on the catalytic activity of the tested composites. The main purpose of the study was to determine the nature of Cu-support interactions, and therefore, to find out what causes the greater or lesser catalytic activity of individual tested systems.

Experimental

Synthesis of materials

A series of CuO-support materials were prepared by impregnation of five various materials – ZrO_2, CeO_2, Al_2O_3, $SrTiO_3$ and boehmite (AlO(OH) or more commonly given as γ-Al_2O_3) by copper nitrate solutions. After impregnation materials were dried at 80 °C for 2 h and next, they were calcined at 250 °C for 1 h. The amounts of the $Cu(NO_3)_2$ solution introduced onto the supports were chosen so, that amount of copper after calcination was 1 wt % and 5 wt % in relation to the weight of the support. Two of the supports – aluminium oxide and cerium oxide were commercial materials – TM-DAR by Taimei (99.99%) and ACROS Organics (99.9%), respectively. The others were obtained as follows: ZrO_2 by precipitation with ammonia from zirconyl nitrate solution and then calcination of the precipitate, $SrTiO_3$ by sol-gel method using citric acid [44] and boehmite in hydrothermal methods.

Due to the fact that before the catalytic measurements, all tested materials were reduced (H_2/Ar mixture, temperature 600 °C), which resulted in the formation of copper-support systems, the following nomenclature was adopted in the remainder of the manuscript: Cu-support for the specific material copper oxide - support (e.g. for the material with an assumed amount of 5 wt % copper - respectively 5%Cu-support).

The common part for the first four supports used was their specific surface area, the values of which are given in Table 1. The last – boehmite, one of the most frequently used catalytic supports due to, *inter alia*, the possibility of synthesizing powders with large specific surfaces area, differs from the other supports by over an order of magnitude larger specific surface.

Table 1 – The specific surface area of supports.

Support	Specific surface area/$m^2 \cdot g^{-1}$
ZrO_2	7.30 ± 0.51
Al_2O_3	9.50 ± 0.50
CeO_2	6.28 ± 0.50
$SrTiO_3$	8.88 ± 0.50
AlO(OH)	157.13 ± 1.10

Material characterization methods

The specific surface area of supports was measured using the BET isotherm method on physisorption apparatus Nova 1200e, Quantachrome Inc. Phase composition of composites Cu-support was determined by Rietveld refinement method (HighScore Plus software) from the diffraction data obtained on X'Pert Pro MD (Philips) device. The diffractometer was equipped with a CuKα (λ = 1.5406 Å) X-ray radiation source and measurements were carried out in the range of 2Θ angle from 10 to 90 deg. The FWHM (full width at half maximum) of the reflections, their positions on the diffractogram, and the instrumental line broadening of the reflections were used to estimate the size of the crystallites in crystal phases using the Scherrer formula. We used data from 3 to 5 reflections with the highest intensity per crystal phase in our calculations.

X-ray Photoelectron Spectroscopy analysis (XPS) was performed using the X-ray photoelectron spectrometer Omnicron NanoTechnology with a 128-channel collector. XPS measurements were undertaken in ultra-high vacuum conditions, below 1.1×10^{-8} mbar. Photoelectrons were excited by an Mg-Kα X-ray source with an X-ray anode operated at 15 keV and 300 W. The deconvolution of the obtained spectra was performed using XPSPEAK software.

The microstructure of powders was observed using a scanning electron microscope Nova Nano SEM 200 FEI (Oxford Instruments) coupled with an energy-dispersive X-ray spectrometer (EDAX) which was used for performing a chemical analysis.

Temperature-programmed reduction/temperature-programmed oxidation (TPR/TPOx) measurements were performed on ChemiSorb 2750 apparatus (Micromeritics). Each sample (support powder, CuO - support powder or CuO − reference sample) for these tests was placed in a quartz reactor in the flow of 5% H_2/Ar and 2%O_2/Ar mixtures. The flow rate of gas mixtures was equal to 40 ml min^{-1}. The mass of samples were around 0.4 g except for the reference sample, the mass of which was 0.022 g. During TPR/TPOx measurements, the samples were heated from room temperature up to 800 °C with a heating rate of 10 deg·min^{-1}.

Thermogravimetric measurements (TG) were performed using Netzsch STA 449 F5 Jupiter. The samples were placed into alumina crucible and were heated up to 1000 °C with the heating rate of 5 deg·min^{-1} in an atmosphere of synthetic air. TG method was applied, besides XRD, as an additional method of verifying the presence of carbon in the samples after catalytic tests.

The catalytic tests were carried out using a fixed-bed quartz reactor at atmospheric pressure. These measurements were performed in the temperature range from 500 to 800 °C (heating cycle) and from 800 to 500 °C (cooling cycle) with 1 h of heating at 800 °C in between. The heating rate was set at 1 °C/min. Before starting the actual measurements, all samples were reduced at 600 °C for 2 h in the stream of hydrogen. Hydrogen was supplied from the electrolyser while other gases were provided by Air Liquide with purity over 99.9%. The gas mixture simulating biogas composition: 65% CH_4 and 35% CO_2 (vol. %) at flow rate of 30 ml/min (18,000 ml_STP g_cat^{-1} h^{-1}; GHSV = 13,329 h^{-1}) was introduced into the reactor and the exhaust gases were examined using PerkinElmer Spectrum 100 FT-IR spectrometer connected directly to the reactor outlet and equipped with heated gas sample cell and the cold trap for H_2O vapour removal. The concentrations of the specific outcoming gases (CH_4, CO_2, CO) were calculated based on the areas under bands (specific fragments) of registered spectra and the calibration curves appropriated for this FTIR-based unit. A detailed description of the set-up can be found elsewhere [45]. In order to estimate the activity of the investigated methane dry reforming catalysts in tested substrate system (65% vol. CH_4 + 35% vol. CO_2) the degrees of CO_2 and CH_4 conversion (in %) in the tested temperature range were calculated and the selectivity towards CO creation was also established. The conversion of CO_2 (X_{CO2}) and CH_4 (X_{CH4}) were determined according to the following equations (Eqn. (6) and (7)):

$$X_{CH_4}(\%) = \frac{F_{CH_4\,in} - F_{CH_4\,out}}{F_{CH_4\,in}} \cdot 100 \tag{6}$$

$$X_{CO_2}(\%) = \frac{F_{CO_2\,in} - F_{CO_2\,out}}{F_{CO_2\,in}} \cdot 100 \tag{7}$$

Selectivity towards CO generation was determined according to Eq. (8) with respect to the amount of CO formed during the reaction to the overall amount of carbon bearing molecules that were converted.

$$S_{CO}(\%) = \frac{F_{CO\,out}}{\left(F_{CH_4\,in} - F_{CH_4\,out}\right) + \left(F_{CO_2\,in} - F_{CO_2\,out}\right)} \cdot 100\% \tag{8}$$

In the equations formulae the $F_{x\,in}/F_{x\,out}$ are the molar flow rates of CH_4, CO_2 or CO in feed (in)/effluent (out) mixture, respectively.

Results and discussion

The phase compositions of both pure support samples and composite materials (supports with an active phase after calcination of the copper precursor) were determined using X-ray diffraction measurements. The results of the analysis of the support samples were shown in Fig. 1. They indicated that the only components were the assumed phases of the oxide systems, both in the case of commercial materials and those synthesized in a laboratory. Sequentially: ZrO_2 support mainly (95 wt %) contained the monoclinic phase of zirconia (ICSD 98-009-4886) and about 5 wt % of the tetragonal ZrO_2 phase (ICDD 01-079-1769); CeO_2-support consisted of cubic CeO_2 phase (ICSD 98-015-7419); Al_2O_3 entirely as α-Al_2O_3 phase (ICDD 01-074-0323); $SrTiO_3$ as tausonite (ICSD 98-009-4573). In the case of AlO(OH) (often referred to as γ-Al_2O_3 phase) the only phase was amorphous boehmite. After impregnation by copper nitrate and calcination apart from the presence of copper oxide CuO (ICSD 98-003-1059) in most materials, only in the case of the composite with $SrTiO_3$ as the support, a small amount of additional phase - TiO_2 also appeared in the system. The phase composition of composite materials was presented in Table 2. As was expected, the amounts of CuO phase are definitely lower in the case of samples with a lower assumed copper content (ultimately 1 wt %) than the amount of copper oxide in these materials with a higher (5 wt %) assumed
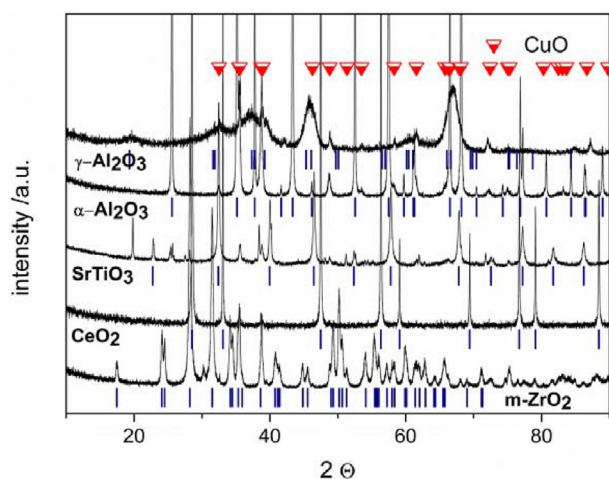
Fig. 1 – The diffractograms of 5%Cu-support samples.

Table 2 – Phase composition of composite samples after calcination.

Sample		Phase composition	Crystallite sizes from diffraction data/nm
ZrO_2	1% Cu	100% ZrO_2	25 ± 4
	5% Cu	89.6% ZrO_2	30 ± 2
		10.4% CuO	44 ± 8
CeO_2	1% Cu	100% CeO_2	207 ± 16
	5% Cu	93.1% CeO_2	209 ± 15
		6.9% CuO	74 ± 14
$SrTiO_3$	1% Cu	95.8% $SrTiO_3$	65 ± 11
		4.2% TiO_2	84 ± 20
	5% Cu	89.7% $SrTiO_3$	59 ± 11
		3.3% TiO_2	95 ± 2
		7.0% CuO	17 ± 3
Al_2O_3	1% Cu	99.3% α-Al_2O_3	130 ± 8
		0.7% CuO	37 ± 7
	5% Cu	93.2% α-Al_2O_3	128 ± 8
		6.8% CuO	24 ± 3
AlO(OH)	1% Cu	AlO(OH)	cannot be determined
		CuO	cannot be determined
	5% Cu	AlO(OH)	cannot be determined
		CuO	57 ± 20

amount. Moreover, in the case of two samples - 1%Cu–ZrO_2 and 1%Cu–CeO_2, the resolution of the X-ray diffraction method did not allow for confirmation of the presence of copper. In the case of these samples, the presence of Cu was identified by energy-dispersive X-ray spectroscopy (EDS) method during observation of the microstructure of composites using a scanning electron microscope. Furthermore, the reflections of copper oxide are clearly visible on the diffraction patterns of all materials where the amount of copper introduced was set as 5 wt %, even in the case of Cu-boehmite material, where diffractogram corresponds rather to the amorphous phase. The diffractograms for series 5%Cu-support were presented on Fig. 1.

It should be added that the values given in Table 2 are subject to a large measurement error, resulting from both – the XRD measurement method itself and the specificity of tested materials. The nature of prepared composites (nanocrystalline materials) causes reflections on the diffractograms

blurred, which deteriorates the accuracy of quantitative interpretation. A particularly difficult case in this respect is the Cu–AlO(OH) amorphous materials for which the quantitative analysis would be completely unreliable, therefore Table 2 does not provide the values for these systems.

Crystallite sizes for the main phases identified in the obtained materials were estimated on the basis of the half-width of the diffraction peaks, which are also given in Table 2. The microstructure of composites (impregnated and calcinated powders) was observed by scanning electron microscope (Fig. 2). One can conclude that tested powders differ more or less significantly from each other. There is a composite with cerium oxide as a support, the microstructure of which is completely different from the other ones - the picture shows oblong structures that indicate the directional growth of the cerium oxide grains. These grains are definitely larger than grains of other supports. Similar effect was found in the case of sizes of CeO_2 crystallites (Table 2).

The remaining powders consist of spherical grains: in the case of the Cu–$SrTiO_3$ composite, they are mostly single grains, while Cu–Al_2O_3 powder consists of agglomerates of several grains, whereas Cu–ZrO_2 composite consists of much larger agglomerates but with smaller grains than in the composites mentioned above. In addition, in the case of Cu–Al_2O_3 one can observe the areas with a different morphology: the vast majority of areas (labelled 2 on Fig. 2) consist of agglomerates of grains with a size of several dozen nanometers but locally can be seen the larger elliptical elements (point 1 in Fig. 2). EDS point analysis carried out for 5%Cu–Al_2O_3 material shows that these areas are significantly enriched in copper (in point 1: Cu - 57 at.%, O - 34 at.%, Al - 9 at.%) compared to most areas (as in point 2: Cu - 1 at.%, O – 49.5 at.%, Al – 49.5 at.%), where there is too little copper in terms of the amount assumed.

In the case of Cu–AlO(OH) composite, which in terms of structure is practically an amorphous system, the grain sizes are by far the smallest, compared to sizes in other powders, and the whole material is inhomogeneous in terms of microstructure.

Despite different microstructure of the oxide and perovskite supports (ZrO_2, CeO_2, $SrTiO_3$ and Al_2O_3), the values of the specific surface area of these materials (obtained from BET measurements – see Table 1) indicate that they do not differ in this respect. Additionally, although the microstructure of Cu–AlO(OH) material seems to be similar to the microstructure of Cu–ZrO_2 material, the specific surface area values are over an order of magnitude higher for this one than for ZrO_2 support and others. The decisive factor here seems to be the amorphous nature of the AlO(OH) support.

All materials presented above were tested by temperature-programmed reduction and oxidation methods (TPR/TPOx) to determine of the potential of a material to participate in redox reactions. Information about this type of property is crucial for materials intended to participate in catalytic processes because it indicates the possibility of fast electron transfer by material components. The research was carried out according to the following scheme: 1) first reduction (I TPR) from room temperature to 900 °C, 2) cooling in helium atmosphere, 3) oxidation (I TPOx), again room temperature – 900 °C, 4) cooling in helium and 5) second reduction from room temperature
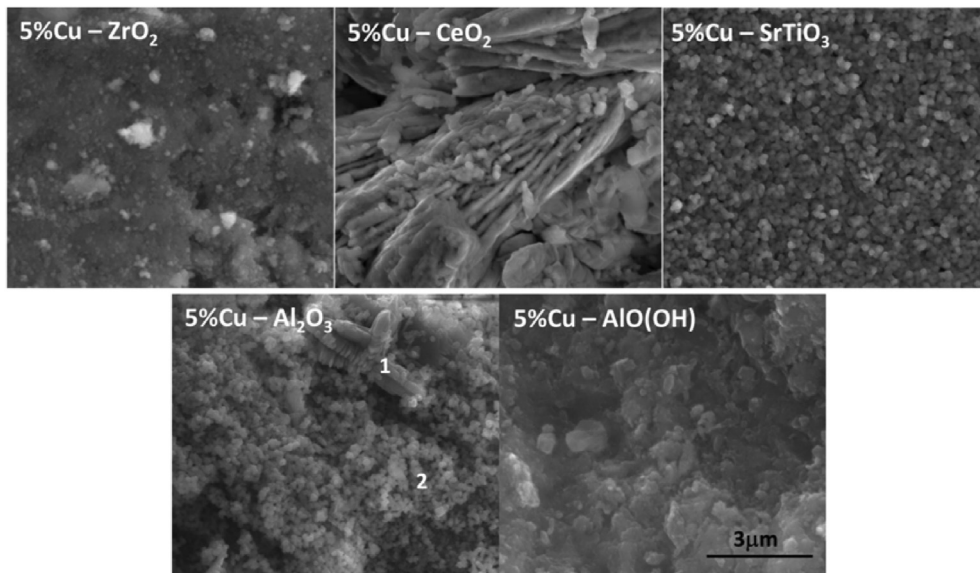
Fig. 2 — Micrographs of 5%Cu − support materials with markers for 5%Cu−Al₂O₃ sample (points 1 and 2) in which EDS analysis was conducted.

to 900 °C (II TPR). The figures presented below show the reduction profiles corresponding to the second reduction (II TPR) for all obtained materials. Maxima on the reduction profiles should be related to the reduction of copper oxide (this effect should be visible for all tested materials) and to the reduction of the support if there is a possibility of reduction of this material with hydrogen in the tested temperature range. Fig. 3 shows the reduction profiles for the reference CuO sample and for all tested composite Cu-support materials, both those with a target content of 1 wt% and 5 wt% of copper. TPR test performed for the reference sample - pure CuO obtained from thermal decomposition of copper (II) nitrate, shows that reduction of copper(II) oxide starts at a higher temperature than for all Cu-support materials even by about 80−100 °C. The reduction of pure copper(II) oxide finishes at around 320 °C, similar to composite materials. The comparison of the reduction profiles of Cu-support materials with lower and higher copper content leads to the conclusion that in both cases, for most materials, reduction peaks appear in similar temperature ranges, only in the case of the Cu−AlO(OH) material, both profiles (for materials with 1%Cu and 5%Cu) differ from the others. In the temperature range from *c.a.* 70 °C to 350 °C (depending on the material), reduction maxima is corresponding to the reduction of copper oxide deposited on supports. The observed maxima are complex, most likely, due to the two-step reduction of copper oxide: $CuO \rightarrow Cu_2O \rightarrow Cu$. In the case of two materials: Cu−SrTiO₃ and Cu−CeO₂, there are also maxima of lower intensity at higher temperatures, in the ranges of 480−560 °C and approx. 420−550 °C, respectively.

In order to identify the process responsible for the effects at higher temperatures and to confirm or deny the possibility of the reduction of support with hydrogen, TPR/TPOx studies of pure supports were carried out. II TPR profiles for pure supports and materials with deposited copper oxide are shown in Fig. 4.

The basic information that can be obtained from these profiles is that in the case of materials with 5% Cu, the target maximums are definitely greater than for materials with 1%
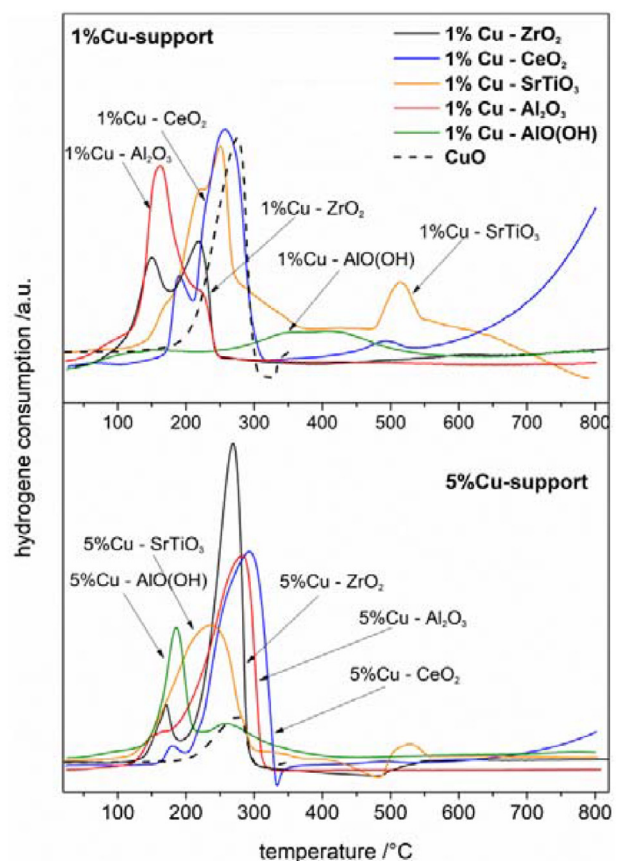
Fig. 3 — II TPR profiles for all obtained materials, solid lines - Cu-support reduction profiles, dashed line - reduction profile of copper(II) oxide.
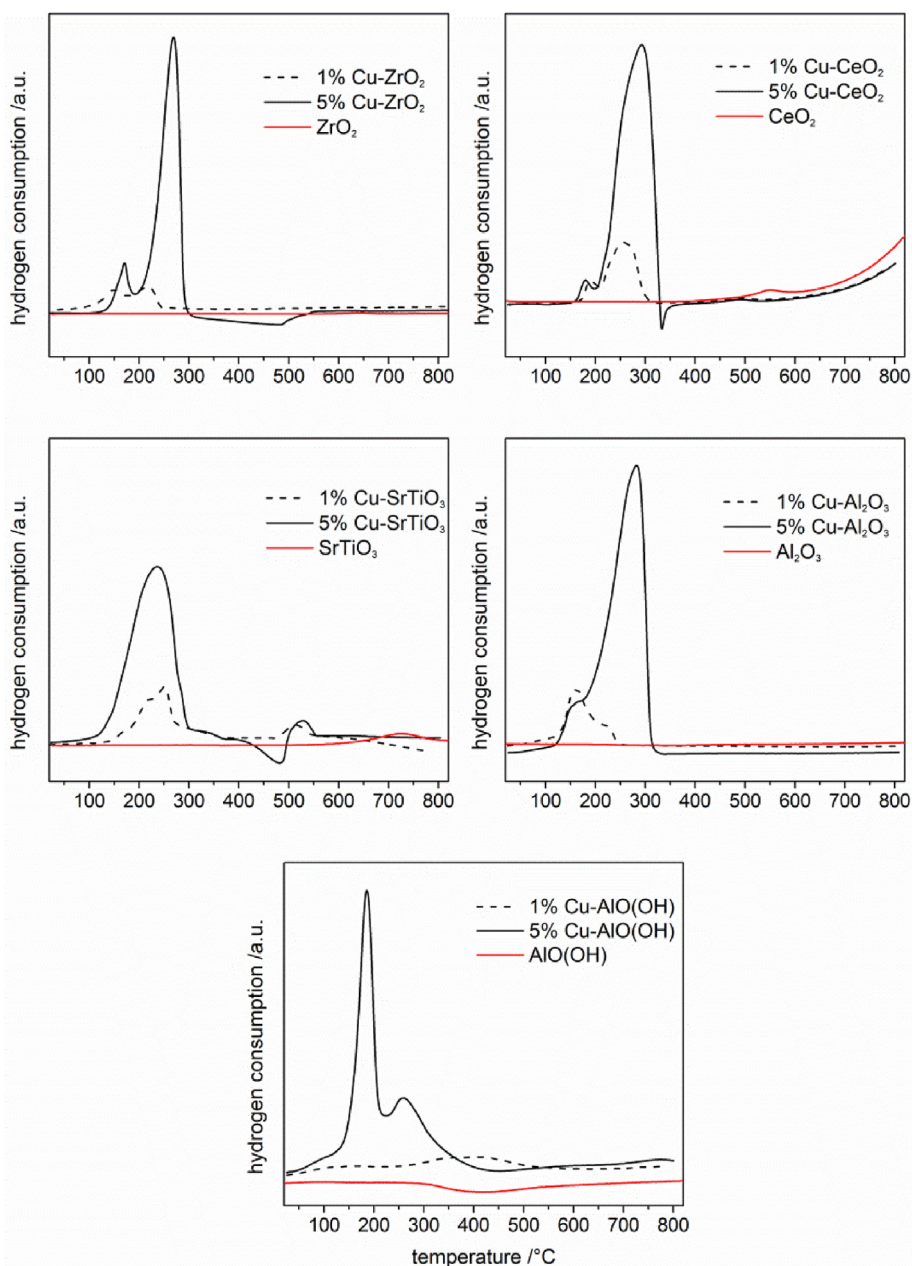
Fig. 4 — II TPR profiles of individual supports and materials with applied copper oxide.

Cu ultimately. This is of course consistent with the assumption because for 5% Cu-support the amount of reduced copper oxide is five times greater. Moreover, it can be seen that maxima in the lower temperature range are complex regardless of the amount of CuO deposited; however, their shape is not identical for materials with more and less copper oxide on the same support. This effect is related not only to the chemical reduction processes but also to physical effects such as the degree of dispersion and the thickness of the coating formed by CuO covering the support. However, TPR profiles presented in Fig. 4 were intended to explain the effects (maxima) that appear in some cases (Cu—CeO₂ and Cu—SrTiO₃) in a higher temperature range. In the case of CeO₂ support, one can observe some slight reduction effect in the temperature range 500—600 °C which is associated with the reduction of

cerium(IV) to cerium(III). The temperature of this process mainly depends on the size of the oxide grains and the grain size distribution, therefore in other papers, one can find various ranges of temperatures for the reduction of cerium(IV) oxide with hydrogen from 400 °C, up to 800 °C [46—48]. Moreover, in the case of CeO₂ as support for CuO a slight elevation with a maximum of about 500 °C on the TPR profile for the 1% Cu—CeO₂ material can be seen (Fig. 3). This effect is no longer visible for 5%Cu—CeO₂ material due to the much more intense effect associated with the reduction of CuO (on this scale, the high-temperature effect "disappears"). In the case of SrTiO₃ support, the small reduction effect above 600 °C, most likely related to the reduction of titanium (IV) to titanium (III), can be noticed. For Cu—SrTiO₃ composites, there is no reduction peak in the same temperature range, but one can observe a

significant reduction effect from around 480 °C–550 °C. TPR/TPOx studies for strontium titanate doped with nickel or chromium, presented in previous papers [13,22,49], indicate that in a similar temperature range there is a reduction of the metal introduced into B sublattice of strontium titanate. Thus, it can be hypothesized that this effect is related to the reduction of copper introduced in the titanium sublattice in $SrTiO_3$ structure. Moreover, the observed effect is an interesting result, because it shows that copper is being incorporated into the $SrTiO_3$ structure even at low temperatures (copper nitrate calcination was performed only at 250 °C). For Cu–AlO(OH) materials two different TPR profiles depending on the amount of CuO applied were obtained. It turns out that in the case of 1%Cu–AlO(OH), only a slight line elevation in the range of 320–500 °C is observed which is a practically insignificant effect compared to the reduction of other composites with the same amount of copper introduced. In this case, we suspect the reaction of copper with the support resulted in the formation of a stable product (possibly the formation of copper hydroxide, copper oxide hydroxide or copper aluminate). These phases are not visible on the diffractograms obtained for the Cu–AlO(OH) system, which proves that they occur in small amounts (below the resolution of the XRD method). Taking into account the results of the work of other Authors who observed the presence of the aluminate phase ($CuAl_2O_4$) in the Cu/γ-Al_2O_3 system and described its reduction at temperatures similar to those presented in this manuscript for the Cu–AlO(OH) [50], we suspect that this phase was created during thermal treatment of Cu–AlO(OH) material. According to Bahmanpour et al. [51] the presence of $CuAl_2O_4$ phase act as strong CO_2 adsorption site however, at the same time, the formation of the spinel phase results in a significant reduction in the specific surface area of the catalyst through the sintering effect. The formation of the aluminate phase in the case of the Cu–AlO(OH) system is much more likely than in Cu–Al_2O_3 system because the boehmite phase is an almost amorphous (and metastable phase), and what is more, it is characterized by an order of greater specific surface area compared to the α-Al_2O_3 support. TPR profile of the 5%Cu–AlO(OH) composite is much more similar to the reduction profiles of other composites - the observed maxima correspond to the CuO reduction.

Compared to TPR profiles of other composites, in this case first maximum is exceptionally high. Thus we assume that for Cu–AlO(OH) material copper oxide is extremely well dispersed on the support material. It is consistent with the previously provided information that specific surface area of AlO(OH) support is an order of magnitude greater related to the other supports. TPR profiles of composites based on Al_2O_3 and ZrO_2 materials are similar and indicate only reduction of copper oxide, which goes in the range 100–320 °C. The presented results of TPR measurements prove that obtained materials have the potential to be used as catalysts for reactions occurring with electron exchange. However, on the basis of the TPR results, it cannot be estimated which of the obtained materials will show the highest catalytic activity in redox reactions. It is necessary to perform the tests in a specific catalytic reaction.

The obtained composites containing copper oxide as the catalytically active phase were examined in the reaction of dry methane reforming DRM ($CH_4 + CO_2 = 2H_2 + 2CO$). Tests were carried out both for materials with 1 wt % of Cu and for materials with 1 wt % of Cu. The results of these tests are summarized and presented (in Fig. 5) as the concentration of CO (reforming product) in the function of temperature, both for the measurement carried out during the temperature increase and decrease. As can be seen, in both series of materials the Cu–ZrO_2 composite showed the lowest catalytic activity. Similarly, it can be concluded that Cu–AlO(OH) material shows the highest catalytic activity. Cu–$SrTiO_3$ and Cu–CeO_2 materials show intermediate, albeit high catalytic activity both in composites with lower and higher copper content. In the case of Cu–$SrTiO_3$ system, such good performance is due to the high dispersion of copper achieved thanks to the incorporation of copper (probably on different oxidation states) into the structure of $SrTiO_3$. The behavior of the Cu–Al_2O_3 material is somewhat surprising - in the case of the 1%Cu–Al_2O_3 composite, the catalytic activity is similar to or even slightly higher than 1%Cu–AlO(OH), while in the 5%Cu–Al_2O_3 system it turns out to be a much less effective catalyst. Thus, it seems that the rational explanation for such a low catalytic activity of 5% Cu–Al_2O_3 is a much smaller amount of copper active sites available for reaction gases (Fig. 2 - SEM photos and EDS results indicating the formation of large, separate clusters of CuO in this material) compared to other (homogeneous) materials. However, the above considerations do not take into account the possibility of CO formation in other processes that can occur under the conditions used.

The conversion of substrates of DRM reaction in function of temperature, for 5%Cu-support materials as catalyst, is presented in Fig. 6.
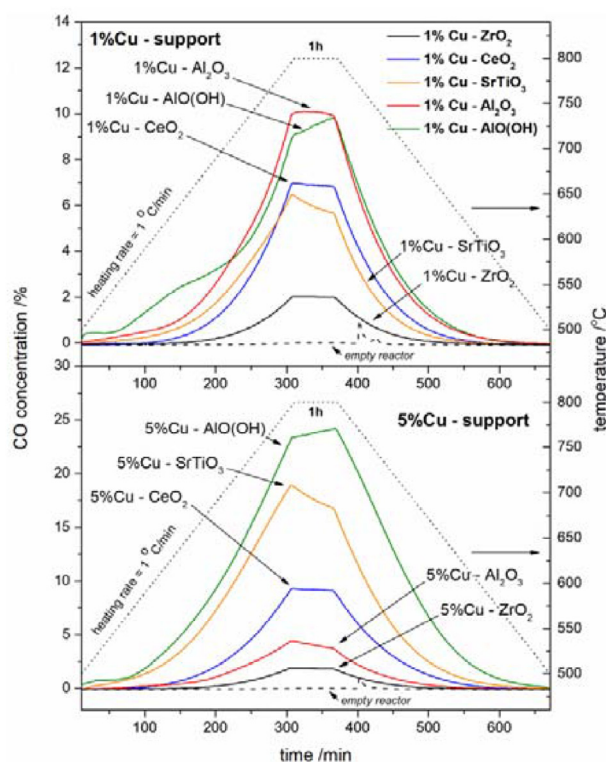

Fig. 5 – The results of catalytic tests for 1%-support and 5%-support as the function of temperature and of process time.
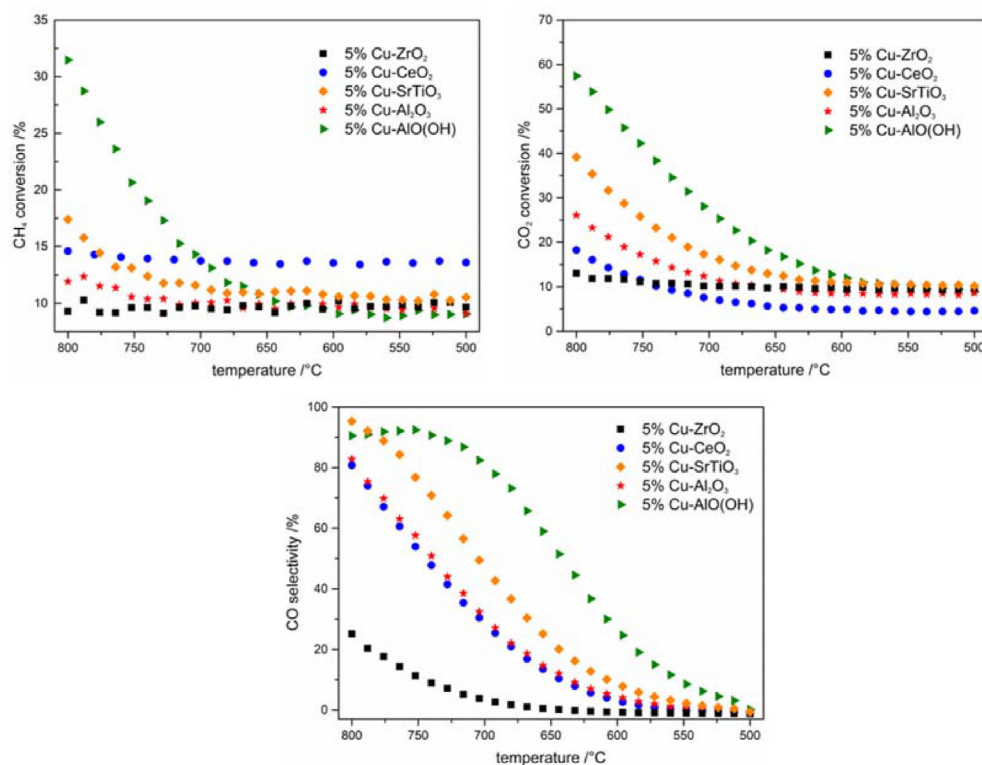
Fig. 6 – Degree of CH_4 and CO_2(above) conversion and selectivity to CO(below) for 5%Cu-support in DRM reaction.

The highest conversion of methane was recorded for 5% Cu–AlO(OH) catalyst, and the lowest for 5%Cu–ZrO₂ catalyst, which of course is consistent with data presented in Fig. 5. It can be observed, that values of X_{CO2} are around twice the values X_{CH4} what is an effect of molar ratio (volume ratio) CH_4 and CO_2 in feed mixture. The degree of conversion of both gases can also be influenced, as mentioned earlier, by parallel reactions that can potentially take place in this system. In the case of 5%Cu–AlO(OH) this ratio is very well reflected by the degrees of conversion of methane and carbon dioxide, this relationship is not maintained in the case of other catalysts.

The main reason for the shift to the increasing amount of the CO formed in each of the tests is a reverse Water Gas Shift Reaction (RWGS) taking into account the reaction between CO_2 and H_2 to form the CO and water vapour. The high kinetics of the reaction makes it highly favorable in the proposed testing set-up. As the reaction is keen on reaching quickly the equilibrium point the H_2 uptake is significant and in an environment so enriched with the CO_2 the hydrogen flow at the outlet is negligible. The secondary reactions that could be considered are e.g., Boudouard reaction and CH_4 thermal cracking because they can be the source of the carbon in the studied system.

In order to verify the hypothesis about the presence of carbon in the materials after catalytic tests, diffractometric analysis, and next, the analysis by Rietveld refinement method for all materials was performed (Table 3). For some materials, thermogravimetric tests in the atmosphere of synthetic air were also carried out to verify the results of XRD analysis. TG measurements indirectly indicate the presence of carbon (in the materials after DRM tests), as the decrease in
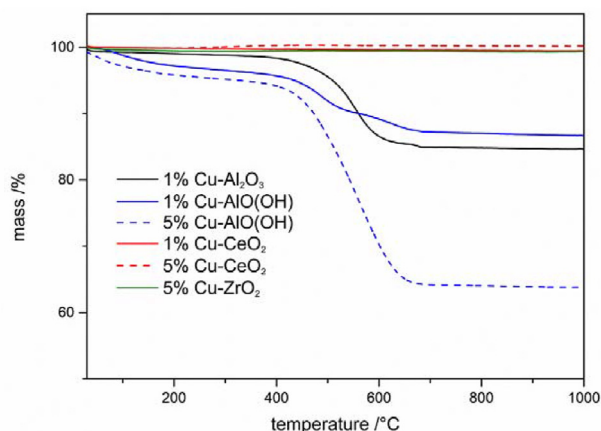
the mass of the material heated in the air atmosphere is the result of the oxidation of carbon to carbon(IV) oxide (Fig. 7).

The results of phase analysis indicated that in the case of only Cu–AlO(OH) and Cu–Al₂O₃ materials the carbon is present after catalytic tests. For Cu–Al₂O₃ samples the Rietveld refinement method indicated specific amounts of graphite however, the determination of a specific amount of carbon phase in the case of Cu–AlO(OH) materials was burdened with a great error due to the large amount of amorphous phase in material (the amount of the carbon phase is not given in the table). Thus, for Cu–AlO(OH) materials, the amount of carbon was estimated on the basis of TG curves and it was 13.3 mass % for 1Cu–AlO(OH) and 35.5 mass % for 5Cu–AlO(OH), respectively. The presence of carbon in the remaining materials (Cu–ZrO₂, Cu–SrTiO₃ and Cu–CeO₂) was also checked using the thermogravimetric method (for selected examples curves on Fig. 7) and the results of these analyzes confirmed the absence of carbon phases in these materials.

The unexpected effect in the case of Cu–SrTiO₃ materials is the presence of strontium carbonate after the catalytic test which is most likely the product of a secondary reaction between CO_2 and the support. Unfortunately, the presence of SrCO₃ phase indicates poor chemical stability of the support in CO_2 atmosphere at high temperatures. Moreover, diffractometric data were used to determine the size of the phase crystallites present in the materials after catalytic tests. Particularly important from the point of view of the catalyst operation is the size of the copper crystallites. As one can see (Table 3), these values are very various: the largest crystallites are found in the case of copper in the Cu–CeO₂ material, half as much for copper in Cu–ZrO₂, and the lowest for the

Table 3 — Phase composition of materials after DRM tests.

Sample		Phase composition after catalytic tests	Crystallite sizes from diffraction data/nm
ZrO_2	1% Cu	100% ZrO_2	28 ± 1
	5% Cu	92.2% ZrO_2	31 ± 2
		7.8% Cu	379 ± 31
CeO_2	1% Cu	100% CeO_2	215 ± 9
	5% Cu	95.4% CeO_2	208 ± 9
		4.6% Cu	>800
$SrTiO_3$	1% Cu	71.7% $SrTiO_3$	68 ± 7
		20.3% TiO_2	101 ± 4
		0.3% Cu	155 ± 22
		7.7% $SrCO_3$	168 ± 3
	5% Cu	76.0% $SrTiO_3$	64 ± 3
		16.9% TiO_2	112 ± 6
		3.5% Cu	132 ± 11
		3.6% $SrCO_3$	101 ± 1
Al_2O_3	1% Cu	85.3% α-Al_2O_3	136 ± 8
		0.5% Cu_2O	20 ± 2
		0.3% Cu	36 ± 5
		13.8% carbon	7 ± 1
	5% Cu	90.3% α-Al_2O_3	132 ± 8
		2.6% Cu_2O	28 ± 2
		2.6% Cu	136 ± 17
		4.5% carbon	11 ± 1
AlO(OH)	1% Cu	AlO(OH)	cannot be determined
		CuO	cannot be determined
		carbon	cannot be determined
	5% Cu	AlO(OH)	cannot be determined
		CuO	cannot be determined
		carbon	cannot be determined

Fig. 7 — Thermogravimetric curves for selected materials after catalytic test.

$Cu-Al_2O_3$ and $Cu-SrTiO_3$ materials. Certainly, in the case of these materials with larger copper crystallites, the specific surface area of the catalytically active material is reduced, which will have a negative impact on the reaction efficiency. The crystallite sizes of the support phases practically did not change after the catalytic tests.

From the point of view of the catalytic properties of the tested systems, an important issue is also the selectivity of the tested catalysts to the products of the DRM reaction.

Considering the selectivity of the DRM process to CO (Fig. 6) - the highest is observed in the case of 5%Cu—AlO(OH) and 5%

$Cu-SrTiO_3$ catalyst. In addition, in the case of reaction on 5% Cu—AlO(OH) catalyst, the selectivity to CO is kept above 90% over a much wider temperature range. Anyway, at the temperature of 800 °C, only the catalyst based on zirconia (5% Cu—ZrO_2) shows a low selectivity to CO (less than 30%).

The obtained results of the catalytic tests, in particular, the one proving the surprisingly low catalytic activity of the Cu—ZrO_2 system in the DRM reaction, prompted the authors to undertake further research on the Cu-support systems. While in the case of the 5%Cu—AlO(OH) system, high catalytic activity can be primarily related to the largest specific surface area of the support (thus the largest catalyst surface available for reaction gases), in the case of 5%Cu—ZrO_2, the surface of the support was comparable to the specific surface of the remaining supports based on which the Cu-support catalysts were obtained. Therefore, it was assumed that the observed catalytic effect must also result from the interactions between copper and support and, most likely, from the possibility of copper taking not only +2 but also at +1 oxidation state. The influence of Cu presence in both oxidation states on reduction-oxidation processes has already been discussed by Chatterjee et al. [43] who noticed that the presence of Cu^+- O species, formed as a result of the copper-support interactions, increases the catalytic activity of the material relative to this reaction.

As was mentioned earlier, X-ray diffraction tests of Cu-support materials indicate that the only phase derived from copper among the tested systems is CuO oxide, while TPR tests show that Cu_2O oxide is most likely present. Moreover, in the case of CeO_2 and $SrTiO_3$ — based catalysts (as indicated in TPR measurements) copper was also partially incorporated into the structure of these supports. In order to confirm the presence of copper on various oxidation states, X-ray Photoelectron Spectroscopy measurements were carried out. The XPS outcome signal intensity was not sufficient to obtain reliable results for series of catalysts with 1% Cu, thus only 5% Cu-support materials were tested (Fig. 7). The detailed analysis of XPS spectra has shown the presence of copper in at least two oxidation states in three materials: Cu—CeO_2, Cu—Al_2O_3 and Cu—AlO(OH). An additional Al—O—Cu solid solution could be most likely identified in the case of Cu—Al_2O_3 and Cu—AlO(OH). The possible creation of $CuAl_2O_4$ spinel oxide is very likely to happen at the interface between Al and Cu species as was mentioned earlier, in the part concerning TPR measurements. In the context of the XPS measurement results, the results of the catalytic tests become more understandable. In the case of Cu—AlO(OH) and Cu—Al_2O_3 systems, their high catalytic activity results most probably due to the simultaneous presence of copper at +2 and + 1 oxidation states. The lower intensity and resolution of the Cu2p collected spectra come from low surface concentration of accessible Cu species. It implies that Cu tends to easily penetrate and diffuse into Al-based substrate materials. The more nonreactive oxide, the more intensive the signal. A similar behaviour was observed for CeO_2 sample due to the notable Cu solubility limit in the ceria lattice. The deconvolution of the Cu2p XPS spectra of AlO(OH) based catalyst gave two main peaks coming from Cu^{2+} (933.8 eV) and Cu^+ (932.6 eV) while for Al_2O_3 sample the corresponding peaks were located at 933.2 eV and 932.3 eV for Cu^{2+} and Cu^+,

respectively. The 2p doublets were separated by 19.9 eV in both cases. The $Cu2p_{3/2}$ peak located at 935.5 eV was assigned to the Cu—O—Al solid solutions that most probably formed during the Cu precursor decomposition. Although, the nearby binding energy region of $Cu(OH)_2$ could also describe the $Cu2p_{3/2}$ located at 935.5 eV. In that case, the spectra analysis is unclear, but the existence of mixed Al—Cu oxide is highly probable when Al_2O_3 is used. This type of spinel structure is likely to be formed and is considered a good CO_2 reduction catalyst although suffering from the low specific surface [51]. According to Arjmand et al. [52] the spinel activity is related to the possibility of its reduction to the $CuAlO_2$, thus, the presence of Cu^{2+} and Cu^+ in alumina-based structure (as $Cu-Al_2O_3$ as Cu—AlO(OH)) during TPR/TPOx cycles is expected. Actually,

a high level of the Cu dissolution was observed in 1% Cu—AlO(OH) sample as the H_2-TPR studies revealed an enormous increase in reduction temperature. Fig. 8.

This behaviour is being observed for Cu—Al—O phases which are harder to reduce than Cu oxides. In that case, the spectra analysis is unclear, but the existence of mixed Al—Cu oxide is highly probable when Al_2O_3 is used. This type of spinel structure is likely to be formed and is considered as good CO_2 reduction catalyst although suffering from low specific surface [51].

Only for the material 5%Cu—Al_2O_3 a decrease in activity was observed, resulting from the inhomogeneous distribution of copper oxide in the material and the formation of its large clusters. In addition, it seems that effect related to a much
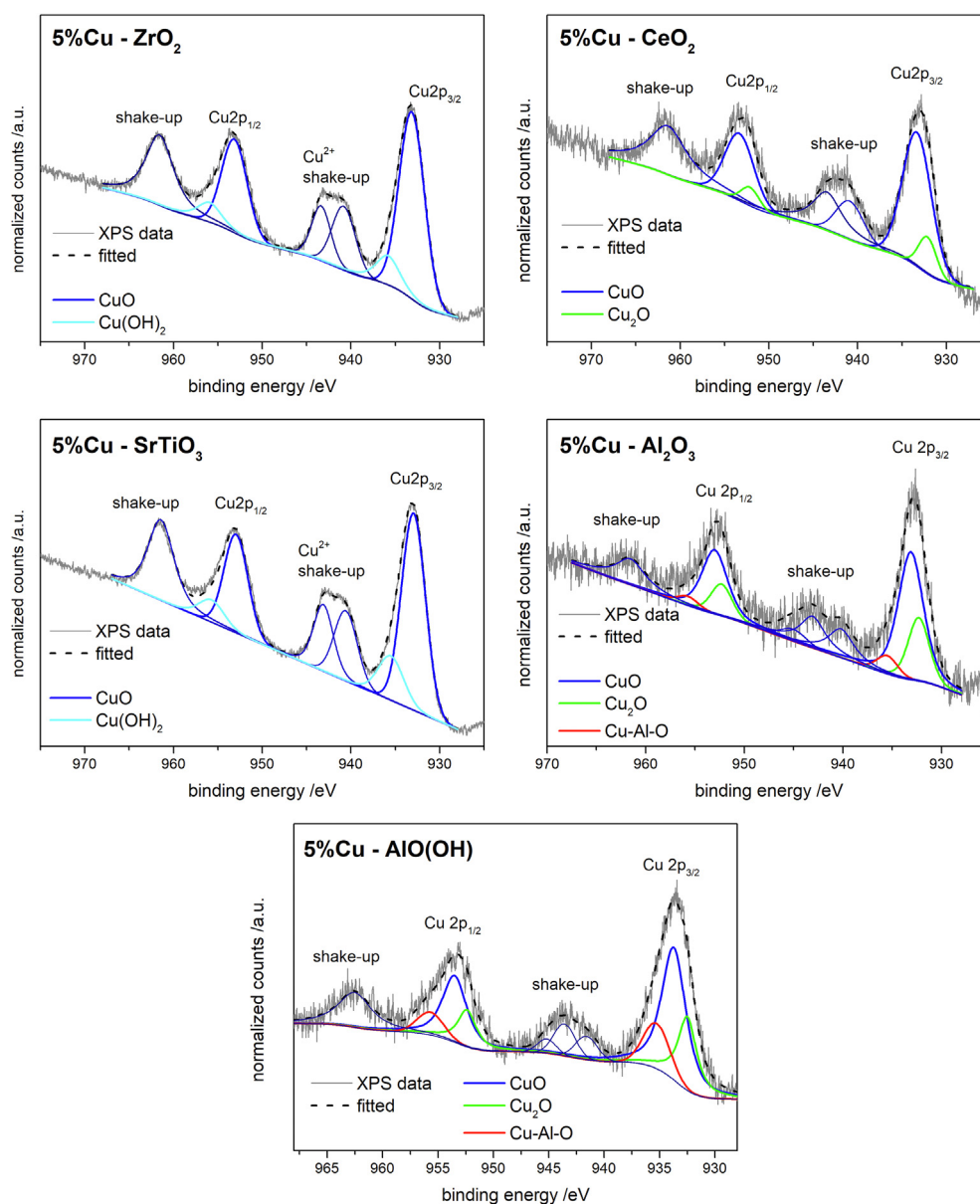

Fig. 8 — Cu2p XPS deconvoluted spectra for samples with 5% Cu additive.

Table 4 – The comparison of catalytic tests results in DRM reaction for nickel and copper catalysts.

Catalyst	Active metal content/wt. %	Preparation of catalyst	T °C	X_{CH4}%	X_{CO2}%	BET m^2g^{-1}	Ref.	Reactor
Ni/α-Al$_2$O$_3$	10 (Ni)	IWIM	550	8.4	34.7	3.3	[54]	FBR
Ni/γ-Al$_2$O$_3$	10 (Ni)	IWIM	550	8.7	36.6	150		
Ni/γ-Al$_2$O$_3$	5 (Ni)		700	7.0	19.5	212	[55]	
Ni/CeO$_2$	10 (Ni)	IWIM	550	11.7	29.7	5.9	[54]	FBR
Ni/ZrO$_2$	5 (Ni)	IWIM	750	74	87	–	[56]	FBR
Ni/Ce$_{0.8}$Zr$_{0.2}$O$_2$	15 (Ni)	Co-precipitation	800	78	77	97	[57]	FBR
Ni–Cu-LDO	1 (Cu)	Co-precipitation	800	95	92	79	[58]	FBR
	5 (Cu)			95	91	78		
La$_{0.8}$Sr$_{0.2}$Ni$_{0.8}$Cu$_{0.2}$O$_3$	5.4 (Cu)	Sol-gel	700	88	86	9.0	[59]	microreactor
OUR/THIS WORK								
Cu/ZrO$_2$	5 (Cu)	IWIM	800	9	12	7.3	–	FBR
Cu/CeO$_2$	5 (Cu)	IWIM	800	14	18	6.3	–	FBR
Cu/SrTiO$_3$	5 (Cu)	IWIM	800	17	39	8.9	–	FBR
Cu/Al$_2$O$_3$	5 (Cu)	IWIM	800	13	26	9.5	–	FBR
Cu/AlO(OH)	5 (Cu)	IWIM	800	33	58	157	–	FBR

X_{CH4} – conversion of methane, X_{CO2} – conversion of carbon dioxide.
LDO – layered double oxides, IWIM – incipient wetness impregnation, FBR – fixed-bed reactor.

larger specific surface of the support, in the case of AlO(OH) is of less importance than the effect of the presence of copper in +1 oxidation state.

In the case of ZrO$_2$ and SrTiO$_3$ substrates, characteristic Cu2p spectra for Cu^{2+} species were collected. The shake-up satellite lines in opposite to CeO$_2$, Al$_2$O$_3$ and AlO(OH) were of high intensity which is characteristic for the existence of CuO species on the surface [53]. The Cu2p spectra was deconvoluted into main Cu^{2+} 2p doublet located at 933.3 eV for ZrO$_2$ and 933.1 eV for SrTiO$_3$, respectively. The traces of possible formation of Cu(OH)$_2$ were detected. This was caused most probably during the powder storage due to water vapour uptake. In the case of the Cu–SrTiO$_3$ material, the presence of Cu$^+$ was not confirmed, but it may be due to the lower amount of copper oxides in the form of separate phases - as previously mentioned, a part of the copper was incorporated into the strontium titanate structure. The built-in copper may also be in the SrTiO$_3$ structure partially in the +1 oxidation state. The relatively high, compared to other tested systems, the catalytic activity of Cu–SrTiO$_3$ materials most likely results from the presence of copper in SrTiO$_3$ structure at both oxidation states. It should also be added that the high catalytic activity expected, due to the presence of copper at +2 and + 1 oxidation states, in the case of Cu–CeO$_2$ systems, is not observed. However, taking into account the results of calculations of the size of copper crystallites in these materials (Table 3), it can be concluded that the effect of the reduction of catalytic activity is related to a significant decrease in the active surface of the copper catalyst deposited on cerium oxide.

The results of the catalytic tests described in this work have been compared with the results obtained by other authors for DRM process (in Table 4).

The table does not include literature data for copper catalysts because, as was mentioned in the introduction part, copper is considered in the literature as an additive in a two-component (with nickel) catalyst, not as a proper catalyst. Thus, two-component systems were included for comparison with Ni-support catalyst, one of them being a perovskite (La$_{0.8}$Sr$_{0.2}$Ni$_{0.8}$Cu$_{0.2}$O$_3$) system. As one can notice, the values

of methane or CO$_2$ conversion degree are the highest for complex Ni–Cu systems. Generally, the lowest values were obtained for Ni–Al$_2$O$_3$ and Cu-support systems. However, taking into account the values of X_{CH4} and X_{CO2} for copper catalyst supported on oxides used in fuel cells (above all ZrO$_2$, CeO$_2$ and SrTiO$_3$) it can be stated that Cu–SrTiO$_3$ catalyst has the greatest potential in terms of catalytic activity for use in a DIR-SOFC. The main problem of the Cu–SrTiO$_3$ system is its poor chemical stability confirmed by the appearance of strontium carbonate in the material after catalytic tests. However, this problem requires further, more detailed research.

Conclusions

The work concerns the possibility of using copper deposited on various supports as a catalyst in the DRM reaction. The choice of the supports was mainly dictated by the use of these materials in technologies related to fuel cells. Thus, the catalysts with varying copper content (1 and 5 wt %) were prepared by deposition on several different support oxides and next characterized in terms of structure and microstructure and then subjected to catalytic tests. The conducted preliminary studies of the reducibility of the tested materials (TPR/TPOx) showed a complicated course of reduction processes, especially in the case of materials based on CeO$_2$, SrTiO$_3$ and AlO(OH) - in their case there are also reduction effects at temperatures above the reduction temperatures of pure CuO. Additionally, temperature-programmed reduction profiles (II TPR) suggested the existence of Cu$_2$O phase which was later confirmed by XPS method for all examined samples except SrTiO$_3$. The analysis of XPS spectra and TPR profiles allows us to conclude that the decomposition of the copper precursor most likely results in the formation of mixed Al–Cu oxide, probably the spinel phase of CuAl$_2$O$_4$ in the case of Cu–Al$_2$O$_3$ and Cu–AlO(OH) materials. AlO(OH) and SrTiO$_3$ based catalysts impregnated with 5 wt% of Cu achieved comparable (despite the huge difference in specific surface

area) and highest methane conversion degree and selectivity towards the production of carbon monoxide at 800 °C. Additionally, 5%Cu—AlO(OH) material maintains high selectivity to CO over a wide temperature range. Among catalysts with 5 wt% Cu, the ZrO_2-based sample achieved the lowest CO selectivity.

Surprisingly, while 1 wt % Cu—Al_2O_3 sample shows high catalytic activity, the corresponding sample with higher copper content (5 wt%) has little activity. The probable cause of such effect is the excessive agglomeration of $CuO/Cu_2O/Cu$ particles on the support surface which was observed at SEM microscope. Both in the context of catalytic activity and selectivity, Cu—$SrTiO_3$ materials turned out to be good DRM catalysts, which is most likely related to the partial incorporation of copper into the structure of strontium titanate. This material shows the highest catalytic activity of all tested systems with comparable surface area (only the Cu—AlO(OH) catalyst with an order of magnitude larger surface area was more active).

Based on the obtained results the Cu—$SrTiO_3$ is the most attractive material for DIR-SOFCs to support the direct internal reforming of biogas. It may be applied as an additional, porous, catalytic layer on the anode surface or may form an independent fuel electrode. However, for the later application, few additional investigations on its electrical conductivity and chemical stability in SOFC operating conditions are required.

Declaration of competing interest

The authors declare that they have no known competing financial interests or personal relationships that could have appeared to influence the work reported in this paper.

Acknowledgements

REFERENCES

[1] Maina SCP, Ballarini AD, Vilella JI, de Miguel SR. Study of the performance and stability in the dry reforming of methane of doped alumina supported iridium catalysts. Catal Today 2020;344:129—42. https://doi.org/10.1016/J.CATTOD.2018.11.023.

[2] Özkara-Aydınoğlu Ş, Özensoy E, Aksoylu AE. The effect of impregnation strategy on methane dry reforming activity of Ce promoted Pt/ZrO2. Int J Hydrogen Energy 2009;34:9711—22. https://doi.org/10.1016/J.IJHYDENE.2009.09.005.

[3] Wang HY, Ruckenstein E. Carbon dioxide reforming of methane to synthesis gas over supported rhodium catalysts: the effect of support. Appl Catal A Gen 2000;204:143—52. https://doi.org/10.1016/S0926-860X(00)00547-0.

[4] Ballarini AD, de Miguel SR, Jablonski EL, Scelza OA, Castro AA. Reforming of CH4 with CO2 on Pt-supported catalysts: effect of the support on the catalytic behaviour. Catal Today 2005;107—108:481—6. https://doi.org/10.1016/J.CATTOD.2005.07.058.

[5] da Fonseca RO, Rabelo-Neto RC, Simões RCC, Mattos Lv, Noronha FB. Pt supported on doped CeO2/Al2O3 as catalyst for dry reforming of methane. Int J Hydrogen Energy 2020;45:5182—91. https://doi.org/10.1016/J.IJHYDENE.2019.09.207.

[6] Effendi A, Hellgardt K, Zhang ZG, Yoshida T. Characterisation of carbon deposits on Ni/SiO2 in the reforming of CH4—CO2 using fixed- and fluidised-bed reactors. Catal Commun 2003;4:203—7. https://doi.org/10.1016/S1566-7367(03)00034-7.

[7] Tu X, Whitehead JC. Plasma-catalytic dry reforming of methane in an atmospheric dielectric barrier discharge: understanding the synergistic effect at low temperature. Appl Catal B Environ 2012;125:439—48. https://doi.org/10.1016/J.APCATB.2012.06.006.

[8] Liu H, Wierzbicki D, Debek R, Motak M, Grzybek T, da Costa P, et al. La-promoted Ni-hydrotalcite-derived catalysts for dry reforming of methane at low temperatures. Fuel 2016;182:8—16. https://doi.org/10.1016/J.FUEL.2016.05.073.

[9] Zhu J, Peng X, Yao L, Deng X, Dong H, Tong D, et al. Synthesis gas production from CO2 reforming of methane over Ni—Ce/SiO2 catalyst: the effect of calcination ambience. Int J Hydrogen Energy 2013;38:117—26. https://doi.org/10.1016/J.IJHYDENE.2012.07.136.

[10] Liu D, Lau R, Borgna A, Yang Y. Carbon dioxide reforming of methane to synthesis gas over Ni-MCM-41 catalysts. Appl Catal A Gen 2009;358:110—8. https://doi.org/10.1016/J.APCATA.2008.12.044.

[11] Han K, Yu W, Xu L, Deng Z, Yu H, Wang F. Reducing carbon deposition and enhancing reaction stability by ceria for methane dry reforming over Ni@SiO2@CeO2 catalyst. Fuel 2021;291:120182. https://doi.org/10.1016/J.FUEL.2021.120182.

[12] Wang F, Han K, Xu L, Yu H, Shi W. Ni/SiO2 catalyst prepared by strong electrostatic adsorption for a low-temperature methane dry reforming reaction. Ind Eng Chem Res 2021;60:3324—33. https://doi.org/10.1021/ACS.IECR.0C06020/SUPPL_FILE/IE0C06020_SI_001.PDF.

[13] Choudhary VR, Uphade BS, Mamman AS. Simultaneous steam and CO2 reforming of methane to syngas over NiO/MgO/SA-5205 in presence and absence of oxygen. Appl Catal A Gen 1998;168:33—46. https://doi.org/10.1016/S0926-860X(97)00331-1.

[14] Watanabe H, Okino R, Hanamura K. Structural evolution of carbon deposition on a Ni/YSZ cermet of a SOFC analyzed by soft x-ray XANES spectroscopy. Int J Hydrogen Energy 2019;44:24028—35. https://doi.org/10.1016/j.ijhydene.2019.07.122.

[15] Barroso-Quiroga MM, Castro-Luna AE. Catalytic activity and effect of modifiers on Ni-based catalysts for the dry reforming of methane. Int J Hydrogen Energy 2010;35:6052—6. https://doi.org/10.1016/J.IJHYDENE.2009.12.073.

[16] Sutthiumporn K, Kawi S. Promotional effect of alkaline earth over Ni—La2O3 catalyst for CO2 reforming of CH4: role of surface oxygen species on H2 production and carbon suppression. Int J Hydrogen Energy 2011;36:14435—46. https://doi.org/10.1016/J.IJHYDENE.2011.08.022.

[17] Chatla A, Ghouri MM, el Hassan OW, Mohamed N, Prakash A v, Elbashir NO. An experimental and first principles DFT investigation on the effect of Cu addition to Ni/Al2O3 catalyst for the dry reforming of methane. Appl

Catal A Gen 2020;602:117699. https://doi.org/10.1016/j.apcata.2020.117699.

[18] Song K, Lu M, Xu S, Chen C, Zhan Y, Li D, et al. Effect of alloy composition on catalytic performance and coke-resistance property of Ni-Cu/Mg(Al)O catalysts for dry reforming of methane. Appl Catal B Environ 2018;239:324−33. https://doi.org/10.1016/j.apcatb.2018.08.023.

[19] Lee J, Bae Y, Hong K, Hong J. Comparative evaluation of Ni-based bimetallic catalysts for dry reforming of methane at low temperature: the effect of alloy itself on performance. Int J Energy Res 2022;46:11228−49. https://doi.org/10.1002/ER.7923.

[20] Sagar Tv, Padmakar D, Lingaiah N, Sai Prasad PS. Influence of solid solution formation on the activity of CeO2 supported Ni−Cu mixed oxide catalysts in dry reforming of methane. Catal Lett 2019;149:2597−606. https://doi.org/10.1007/S10562-019-02801-Y. 2019 149:9.

[21] Song K, Lu M, Xu S, Chen C, Zhan Y, Li D, et al. Effect of alloy composition on catalytic performance and coke-resistance property of Ni-Cu/Mg(Al)O catalysts for dry reforming of methane. Appl Catal B Environ 2018;239:324−33. https://doi.org/10.1016/J.APCATB.2018.08.023.

[22] Rahemi N, Haghighi M, Babaluo AA, Jafari MF, Khorram S. Non-thermal plasma assisted synthesis and physicochemical characterizations of Co and Cu doped Ni/Al2O3 nanocatalysts used for dry reforming of methane. Int J Hydrogen Energy 2013;38:16048−61. https://doi.org/10.1016/J.IJHYDENE.2013.08.084.

[23] Zhang J, Wang H, Dalai AK. Development of stable bimetallic catalysts for carbon dioxide reforming of methane. J Catal 2007;249:300−10. https://doi.org/10.1016/J.JCAT.2007.05.004.

[24] Sutthiumporn K, Maneerung T, Kathiraser Y, Kawi S. CO2 dry-reforming of methane over La0.8Sr0.2Ni0.8M0.2O3 perovskite (M = Bi, Co, Cr, Cu, Fe): roles of lattice oxygen on C−H activation and carbon suppression. Int J Hydrogen Energy 2012;37:11195−207. https://doi.org/10.1016/J.IJHYDENE.2012.04.059.

[25] Bian Z, Zhong W, Yu Y, Jiang B, Kawi S. Cu/SiO2 derived from copper phyllosilicate for low-temperature water-gas shift reaction: role of Cu+ sites. Int J Hydrogen Energy 2020;45:27078−88. https://doi.org/10.1016/J.IJHYDENE.2020.07.054.

[26] Mizera A, Kowalczyk A, Chmielarz L, Drożdż E. Catalysts based on strontium titanate doped with Ni/Co/Cu for dry reforming of methane. Materials 2021;14:7227. https://doi.org/10.3390/MA14237227. 2021;14:7227.

[27] Foppa L, Margossian T, Kim SM, Copéret C, Larmier K, et al. Contrasting the role of Ni/Al2O3 interfaces in water-gas shift and dry reforming of methane. J Am Chem Soc 2017;139:17128−39. https://doi.org/10.1021/JACS.7B08984/SUPPL_FILE/JA7B08984_SI_002.ZIP.

[28] li Xu L, Wen H, Jin X, Bing Q ming, Liu J yao. DFT study on dry reforming of methane over Ni2Fe overlayer of Ni(1 1 1) surface. Appl Surf Sci 2018;443:515−24. https://doi.org/10.1016/J.APSUSC.2018.02.268.

[29] Chen S, Zaffran J, Yang B. Dry reforming of methane over the cobalt catalyst: theoretical insights into the reaction kinetics and mechanism for catalyst deactivation. Appl Catal B Environ 2020;270:118859. https://doi.org/10.1016/J.APCATB.2020.118859.

[30] Zhang L, Meng Y, Yang J, Shen H, Yang C, Xie B, et al. Theoretical study on dry reforming of methane catalyzed by Cu12M (M = Cu, Fe, Co, Ni) core-shell bimetallic clusters. Fuel 2021;303. https://doi.org/10.1016/J.FUEL.2021.121263.

[31] Pimenov A, Ullrich J, Lunkenheimer P, Loidl A, Rüscher CH. Ionic conductivity and relaxations in ZrO2−Y2O3 solid solutions. Solid State Ionics 1998;109:111−8. https://doi.org/10.1016/S0167-2738(98)00082-4.

[32] Sasaki K, Maier J. Chemical surface exchange of oxygen on Y2O3-stabilized ZrO2. Solid State Ionics 2003;161:145−54. https://doi.org/10.1016/S0167-2738(03)00264-9.

[33] Bellido JDA, Assaf EM. Effect of the Y2O3−ZrO2 support composition on nickel catalyst evaluated in dry reforming of methane. Appl Catal A Gen 2009;352:179−87. https://doi.org/10.1016/j.apcata.2008.10.002.

[34] Marina OA, Bagger C, Primdahl S, Mogensen M. A solid oxide fuel cell with a gadolinia-doped ceria anode: preparation and performance. Solid State Ionics 1999;123:199−208. https://doi.org/10.1016/S0167-2738(99)00111-3.

[35] Che Abdullah SSB, Teranishi T, Hayashi H, Kishimoto A. Enhanced electrical conductivity of doped CeO2 under millimeter-wave irradiation heating. Mater Des 2017;115:231−7. https://doi.org/10.1016/j.matdes.2016.11.051.

[36] Bochentyn B, Chlipała M, Gazda M, Wang SF, Jasiński P. Copper and cobalt co-doped ceria as an anode catalyst for DIR-SOFCs fueled by biogas. Solid State Ionics 2019;330:47−53. https://doi.org/10.1016/j.ssi.2018.12.007.

[37] Noll F, Münch W, Denk I, Maier J. SrTiO3 as a prototype of a mixed conductor Conductivities, oxygen diffusion and boundary effects. Solid State Ionics 1996;86−88:711−7. https://doi.org/10.1016/0167-2738(96)00155-5.

[38] Suthirakun S, Xiao G, Ammal SC, Chen F, zur Loye H-C, Heyden A. Rational design of mixed ionic and electronic conducting perovskite oxides for solid oxide fuel cell anode materials: a case study for doped SrTiO3. J Power Sources 2014;245:875−86. https://doi.org/10.1016/j.jpowsour.2013.07.040.

[39] Łącz A, Łańcucki Ł, Lach R, Kamecki B, Drożdż E. Structural and electrical properties of Cr-doped SrTiO3 porous materials. Int J Hydrogen Energy 2018;43:8999−9005. https://doi.org/10.1016/j.ijhydene.2018.03.180.

[40] Fichtl MB, Schumann J, Kasatkin I, Jacobsen N, Behrens M, Schlögl R, et al. Counting of oxygen defects versus metal surface sites in methanol synthesis catalysts by different probe molecules. Angew Chem Int Ed 2014;53:7043−7. https://doi.org/10.1002/anie.201400575.

[41] van den Berg R, Prieto G, Korpershoek G, van der Wal LI, van Bunningen AJ, Lægsgaard-Jørgensen S, et al. Structure sensitivity of Cu and CuZn catalysts relevant to industrial methanol synthesis. Nat Commun 2016;7:13057. https://doi.org/10.1038/ncomms13057.

[42] Tiscornia IS, Lacoste AM, Gómez LE, Boix A v. CuO−CeO2/SiO2 coating on ceramic monolith: effect of the nature of the catalyst support on CO preferential oxidation in a H2-rich stream. Int J Hydrogen Energy 2020;45:6636−50. https://doi.org/10.1016/j.ijhydene.2019.12.126.

[43] Chatterjee R, Kuld S, van den Berg R, Chen A, Shen W, Christensen JM, et al. Mapping support interactions in copper catalysts. Top Catal 2019;62:649−59. https://doi.org/10.1007/s11244-019-01150-9.

[44] Drożdż E, Łącz A, Koleżyński A, Mikuła A, Mars K. Experimental and theoretical studies of structural and electrical properties of highly porous Sr1-xYxTiO3. Solid State Ionics 2017;302:173−9. https://doi.org/10.1016/j.ssi.2016.11.014.

[45] Chlipała M, Błaszczak P, Wang S-F, Jasiński P, Bochentyn B. In situ study of a composition of outlet gases from biogas fuelled Solid Oxide Fuel Cell performed by the Fourier Transform Infrared Spectroscopy. Int J Hydrogen Energy 2019;44:13864−74. https://doi.org/10.1016/j.ijhydene.2019.03.243.

[46] Cam TS, Vishnevskaya TA, Omarov SO, Nevedomskiy VN, Popkov VI. Urea−nitrate combustion synthesis of CuO/CeO2 nanocatalysts toward low-temperature oxidation of CO: the effect of Red/Ox ratio. J Mater Sci 2020;55:11891−906. https://doi.org/10.1007/s10853-020-04857-3.

[47] Yao X, Wang Z, Yu S, Yang F, Dong L. Acid pretreatment effect on the physicochemical property and catalytic performance of CeO2 for NH3-SCR. Appl Catal A Gen 2017;542:282–8. https://doi.org/10.1016/j.apcata.2017.06.003.

[48] Kakuta N, Ikawa S, Eguchi T, Murakami K, Ohkita H, Mizushima T. Oxidation behavior of reduced (CeO2)1−x-(ZrO2)x (x=0, 0.2, 0.5) catalysts. J Alloys Compd 2006;408–412:1078–83. https://doi.org/10.1016/j.jallcom.2004.12.134.

[49] Mizera A, Drożdż E. Studies on structural, redox and electrical properties of Ni-doped strontium titanate materials. Ceram Int 2020;46:24635–41. https://doi.org/10.1016/j.ceramint.2020.06.252.

[50] Kwak JH, Tonkyn R, Tran D, Mei D, Cho SJ, Kovarik L, et al. Size-dependent catalytic performance of CuO on γ-Al2O3: NO reduction versus NH3 oxidation. ACS Catal 2012;2:1432–40. https://doi.org/10.1021/cs3002463.

[51] Bahmanpour AM, le Monnier BP, Du Y-P, Héroguel F, Luterbacher JS, Kröcher O. Increasing the activity of the Cu/CuAl2O4/Al2O3 catalyst for the RWGS through preserving the Cu2+ ions. Chem Commun 2021;57:1153–6. https://doi.org/10.1039/D0CC07142K.

[52] Arjmand M, Azad A-M, Leion H, Mattisson T, Lyngfelt A. Evaluation of CuAl2O4 as an oxygen carrier in chemical-looping combustion. Ind Eng Chem Res 2012;51:13924–34. https://doi.org/10.1021/ie300427w.

[53] Biesinger MC, Hart BR, Polack R, Kobe BA, Smart RStC. Analysis of mineral surface chemistry in flotation separation using imaging XPS. Miner Eng 2007;20:152–62. https://doi.org/10.1016/j.mineng.2006.08.006.

[54] Barroso-Quiroga MM, Castro-Luna AE. Catalytic activity and effect of modifiers on Ni-based catalysts for the dry reforming of methane. Int J Hydrogen Energy 2010;35:6052–6. https://doi.org/10.1016/J.IJHYDENE.2009.12.073.

[55] Therdthianwong S, Siangchin C, Therdthianwong A. Improvement of coke resistance of Ni/Al2O3 catalyst in CH4/CO2 reforming by ZrO2 addition. Fuel Process Technol 2008;2:160–8. https://doi.org/10.1016/J.FUPROC.2007.09.003.

[56] Chang JS, Hong DY, Li X, Park SE. Thermogravimetric analyses and catalytic behaviors of zirconia-supported nickel catalysts for carbon dioxide reforming of methane. Catal Today 2006;115:186–90. https://doi.org/10.1016/J.CATTOD.2006.02.052.

[57] Jang WJ, Jeong DW, Shim JO, Roh HS, Son IH, Lee SJ. H2 and CO production over a stable Ni–MgO–Ce0.8Zr0.2O2 catalyst from CO2 reforming of CH4. Int J Hydrogen Energy 2013;38:4508–12. https://doi.org/10.1016/J.IJHYDENE.2013.01.196.

[58] Li B, Xu Z, Jing F, Luo S, Wang N, Chu W. Improvement of catalytic stability for CO2 reforming of methane by copper promoted Ni-based catalyst derived from layered-double hydroxides. J Energy Chem 2016;6:1078–85. https://doi.org/10.1016/J.JECHEM.2016.11.001.

[59] Sutthiumporn K, Maneerung T, Kathiraser Y, Kawi S. CO2 dry-reforming of methane over La0.8Sr0.2Ni0.8M0.2O3 perovskite (M = Bi, Co, Cr, Cu, Fe): roles of lattice oxygen on C–H activation and carbon suppression. Int J Hydrogen Energy 2012;37:11195–207. https://doi.org/10.1016/J.IJHYDENE.2012.04.059.